



## Frequency and temperature dependence behaviour of impedance, modulus and conductivity of $\text{BaBi}_4\text{Ti}_4\text{O}_{15}$ Aurivillius ceramic

Tanmaya Badapanda<sup>1,\*</sup>, Ranjan Kumar Harichandan<sup>2</sup>, Sudhasu Sekhar Nayak<sup>2</sup>, Avinna Mishra<sup>3</sup>, Sahid Anwar<sup>3</sup>

<sup>1</sup>Department of Physics, C.V. Raman College of Engineering, Bhubaneswar, Odisha, 752054, India

<sup>2</sup>Department of Physics, Centurion University of Technology & Management, Bhubaneswar, Odisha, 751020, India

<sup>3</sup>Polytechnics Colloids & Materials Chemistry, Institute of Minerals and Materials Technology, Bhubaneswar, Odisha, 751013, India

Received 8 August 2014; Received in revised form 24 September 2014; Accepted 27 September 2014

### Abstract

*In this work, we report the dielectric, impedance, modulus and conductivity study of  $\text{BaBi}_4\text{Ti}_4\text{O}_{15}$  ceramic synthesized by solid state reaction. X-ray diffraction (XRD) pattern showed orthorhombic structure with space group  $A_{21}am$  confirming it to be an  $m = 4$  member of the Aurivillius oxide. The frequency dependence dielectric study shows that the value of dielectric constant is high at lower frequencies and decreases with increase in frequency. Impedance spectroscopy analyses reveal a non-Debye relaxation phenomenon since relaxation frequency moves towards the positive side with increase in temperature. The shift in impedance peaks towards higher frequency side indicates conduction in material and favouring of the long range motion of mobile charge carriers. The Nyquist plot from complex impedance spectrum shows only one semicircular arc representing the grain effect in the electrical conduction. The modulus mechanism indicates the non-Debye type of conductivity relaxation in the material, which is supported by impedance data. Relaxation times extracted using imaginary part of complex impedance ( $Z''$ ) and modulus ( $M''$ ) were also found to follow Arrhenius law. The frequency dependent AC conductivity at different temperatures indicates that the conduction process is thermally activated. The variation of DC conductivity exhibits a negative temperature coefficient of resistance behaviour.*

**Keywords:** Aurivillius compound, impedance spectroscopy, grain boundary, electric modulus, dielectric relaxation, AC conductivity

### I. Introduction

Aurivillius bismuth-layer structure ferroelectrics pose attractive electrical properties (BLSFs) such as excellent fatigue endurance, fast switching speed, good polarization retention, relatively high Curie temperature, low aging rate and low operating voltage. Due to their excellent properties these materials are commercially applicable as ferroelectric non-volatile random access memory (FRAM) storage devices, high temperature piezoelectric device and sensor applications [1,2]. Bismuth layered structure ferroelectrics belong to a multilayer family of so-called Aurivillius phase with a general chemical formula  $(\text{Bi}_2\text{O}_2)^{2+}(\text{A}_{m-1}\text{B}_m\text{O}_{3m+1})^{2-}$ ,

where A is a combination of one or more mono-, di- and trivalent ions with 12-fold coordinated cation; B is a combination of tetra-, penta-, and hexavalent ions with 6-fold coordinated cation and  $m$  refers to the number of  $\text{BO}_6$  octahedra between neighboring  $\text{Bi}_2\text{O}_2$  layers along the  $c$ -axis [3–5]. These  $\text{BO}_6$  octahedra exhibit spontaneous polarization and  $(\text{Bi}_2\text{O}_2)^{2+}$  layers act as the insulating paraelectric layers and mainly control the electrical response such as electrical conductivity, while the ferroelectricity arises mainly in the perovskite blocks [6]. Majority of these oxides are normal ferroelectrics with fairly high Curie temperatures as a consequence of three main distortions from the prototype high temperature paraelectric phase, namely tilting of octahedra around the  $a$ - and  $c$ -axes and cationic displacement along the polar  $a$ -axis. Very few of these ceramics shows

\*Corresponding author: tel: +91 674 2113593, mob: +91 9437306100, e-mail: badapanda.tanmaya@gmail.com

relaxor behaviour, such as  $\text{BaBi}_2\text{Nb}_2\text{O}_9$ ,  $\text{BaBi}_2\text{Ta}_2\text{O}_9$ ,  $\text{BaBi}_4\text{Ti}_4\text{O}_{15}$  (BBT) etc. [7,8].  $\text{BaBi}_4\text{Ti}_4\text{O}_{15}$  is a  $m = 4$  member of bismuth layered-structured ferroelectric, which shows four slabs of perovskite layers separated by one slab of fluorite layer. BBT has Ba and Bi ions occupying A sites and Ti ions in the B sites of perovskite ( $[\text{A}_{m-1}\text{B}_m\text{O}_{3m+1}]^{2-}$ ) block and it shows a diffuse phase transition from 390 °C to 440 °C.

Impedance spectroscopy is a powerful technique tool for investigation of complex electrical properties. Depending on the chemical composition, various ferroelectric/antiferroelectric or paraelectric phases with slightly different dielectric properties and crystal structures of different type are formed. In all ferroelectrics the study of electrical conductivity is very important to realize the associated physical properties and nature of conductivity in these materials. It is well known that the interior defects such as A site vacancies, space charge electrons or oxygen vacancies have great influence on ferroelectric fatigue or ionic conductivity of the material. Considering that the solid defects play a decisive role in all of these applications, it is very important to gain a fundamental understanding of their conductive mechanism. Various kinds of defects are always suggested as being responsible for the dielectric relaxations at high temperature range. The AC impedance analysis is a powerful tool to separate the grain boundary effects. It is also useful to establish dependence of its relaxation mechanism on the grain and grain boundary effects by considering the different values of resistance and capacitance. The AC impedance is a non-destructive experimental technique for the characterization of micro structural and electrical properties of different electronic material. The technique is based on the analysis of response of a system towards the input AC and the calculation of impedance as a function of the frequency. The frequency dependent properties of a material can be described as complex permittivity ( $\epsilon^*$ ), complex impedance ( $Z^*$ ), complex admittance ( $Y^*$ ), complex electric modulus ( $M^*$ ) and dielectric loss or dissipation factor ( $\tan \delta$ ). The phenomenon of impedance spectroscopy is applied to the dielectric materials, i.e. solid or liquid non-conductors whose electrical characteristics involve dipolar rotation, and to materials with electronic conduction [8,9].

Recently, there have been many reports on the synthesis and characterization of BBT with regard to its structural, dielectric and ferroelectric properties [10–14]. In our earlier work, we have reported the detail structural, ferroelectric and relaxor behaviour with a detailed analysis of relaxor and diffuse behaviour of BBT ceramic [15]. But there are very few reports on the dielectric dispersion and conduction mechanism of BBT ceramic. Recently Kumar *et al.* [16] have reported the dielectric relaxation of BBT ceramics mostly within the ferroelectric region (30–470 °C). In this paper we report the dielectric dispersion and conduction mechanism of BBT ceramics in the paraelectric region (486–786 °C) by

employing the impedance spectroscopy. Electric modulus and the relaxation behaviour have been studied by analysing the complex impedance. The resistivity and capacitance associated with grains were determined.

## II. Experimental details

The stoichiometric ratio of starting chemicals  $\text{BaCO}_3$  (99.9%),  $\text{TiO}_2$  (99.9%) and  $\text{Bi}_2\text{O}_3$  (99.9%) (E. MerckIndia Ltd.) was weighed for the composition  $\text{BaBi}_4\text{Ti}_4\text{O}_{15}$ . The weighed powders were ball milled in a laboratory ball milling machine for 8 h using high purity zirconia balls and acetone as a medium. After drying, calcination was done in a high purity alumina crucible at 1000 °C for 2 h in a conventional programmable furnace. The calcined powders were grinded using an agate mortar and then pressed into discs using pressure of 250 MPa in a hydraulic press with 5 wt.% PVA solution added as a binder. The discs were sintered at 1100 °C for 1 h with 5 °C/min heating rate. The phase purity of the calcined powders was confirmed by the X-ray diffractometer. X-ray diffraction analysis of the samples was carried out using a Philips diffractometer model PW-1830 with  $\text{Cu-K}\alpha$  ( $\lambda = 1.5418 \text{ \AA}$ ) radiation in a wide range of  $2\theta$  ( $20^\circ < 2\theta < 70^\circ$ ) at a scanning rate of 0.5°/min. For electrical measurements, silver electrodes were applied on the opposite disk faces and were heated at 700 °C for 5 min. The frequency (1 Hz–1 MHz) and temperature (486–786 °C) dependent dielectric measurement were carried out using a N4L-NumetriQ (model PSM1735) connected to PC.

## III. Results and discussion

### 3.1. X-ray diffraction

Figure 1 shows the XRD pattern of  $\text{BaBi}_4\text{Ti}_4\text{O}_{15}$  ceramic calcined at 1000 °C for 2 h and sintered at 1100 °C for 2 h. The X-ray diffraction patterns could be indexed as a pure Bi-layered perovskite structure with  $m = 4$ . No impurity peaks corresponding to any other secondary

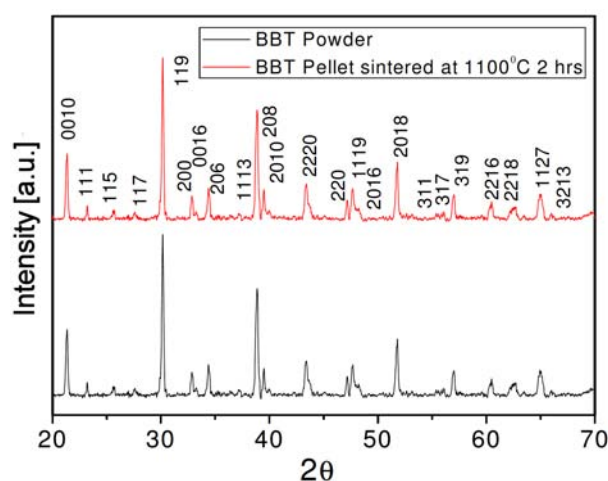


Figure 1. XRD pattern of BBT powder calcined at 1000 °C for 2 h and pellet sintered at 1100 °C for 2 h

phase were found in the XRD patterns which confirms the single phase nature of the compositions. So the obtained phase was indexed using the orthorhombic space group  $A_{21}am$  which is in close agreement with the earlier reports [17–19]. The detail structural analysis and lattice parameters were obtained from Rietveld refinement study which has been reported in our earlier report [16].

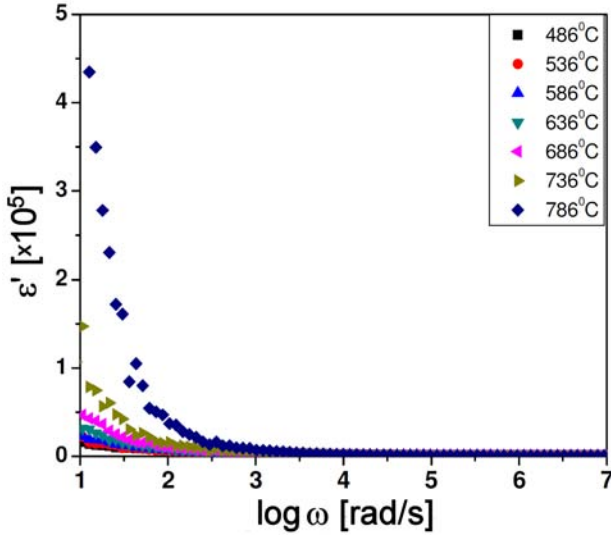


Figure 2. Frequency dependent real part of dielectric constant at different temperatures

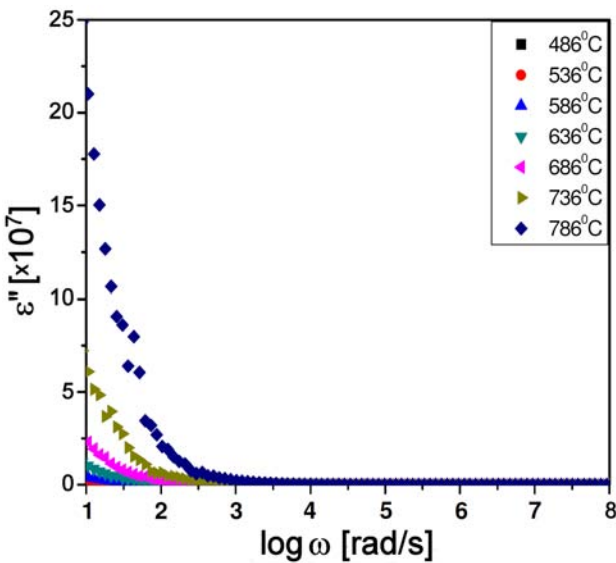


Figure 3. Frequency dependent imaginary part of dielectric constant at different temperatures

### 3.2. Frequency dependence of dielectric study

Figure 2 shows the variation of dielectric constant ( $\epsilon'$ ) of the BBT ceramic at different temperatures as the function of angular frequency ( $\omega = 2\pi f$ ). The frequency dependent complex dielectric permittivity is given by:

$$\frac{\epsilon^* - \epsilon_\alpha}{\epsilon_s - \epsilon_\alpha} = \frac{1}{1 + j\omega\tau} \quad (1)$$

where  $\epsilon_s$  and  $\epsilon_\alpha$  are low and high frequency dielectric constants and  $\tau$  is the time constant. It is observed from Fig. 2 that the dielectric constants sharply decrease with increasing frequency ( $<1$  kHz), and the rate of decrease levels off in a certain frequency range ( $>1$  kHz). But, at relatively low frequency, the dielectric constant strongly depends on frequency, evidently showing a dielectric dispersion [15]. Such a strong dispersion seems to be a common feature in ferroelectric materials concerned with ionic conductivity, which is referred as low-frequency dielectric dispersion. When the frequency increases, the relative effect of ionic conductivity becomes small and as a result, the frequency dependence of dielectric constant becomes weak. At lower frequencies, the dipolar complexes will be able to keep up with the applied field and reorient with each half cycle. The full effect of the polarization reversal will contribute to the dielectric constant [14].

Figure 3 plots the frequency dependence of imaginary dielectric constant  $\epsilon''$  of BBT at various temperatures. Similar to the behaviour of dielectric constant with frequency, the dielectric loss increases with increasing temperature. No loss peak was observed in the  $\epsilon''$  spectra. The high values of  $\epsilon''$  at high temperatures and the large drop of  $\epsilon''$  with increase in frequency seem to indicate the influence of conductivity and space charge polarization. This indicates the thermally activated nature of the dielectric relaxation of the system. The fast rising trend of  $\epsilon''$  at low frequencies may be due to the polarization mechanism associated with the thermally activated conduction of mobile ions and/or other defects. High values of dielectric permittivity are observed only at very high temperature and very low frequencies which is may be due to the free charge build up at interfaces within the bulk of the sample (interfacial Maxwell-Wagner (MW) polarization) [20] and at the interface between the sample and the electrodes (space-charge polarization).

### 3.3. Impedance spectroscopy study

In order to understand the observed dielectric dispersion, we carried out the complex impedance analysis. Figure 4 shows the variation of real part of impedance ( $Z'$ ) with the corresponding frequency at different temperatures. The value of  $Z'$  for all temperatures coincides at high frequency. This behaviour is due to the reduction of barrier with increase in temperature due to which the AC conductivity is increased. At low frequency,  $Z'$  value decreases with rise in temperature indicating the negative temperature coefficient of resistance (NTCR). Figure 5 shows the graph of imaginary parts of impedance  $Z''$  versus frequency at temperatures between 486 °C and 786 °C. The graph showed that  $Z''_{max}$  shifts to higher frequency with the increase in temperature representing a relaxor behaviour within the ceramic [12–14]. A significant broadening of the peaks with increasing temperature suggests the presence of electrical processes in the material with spread of relaxation time. This may

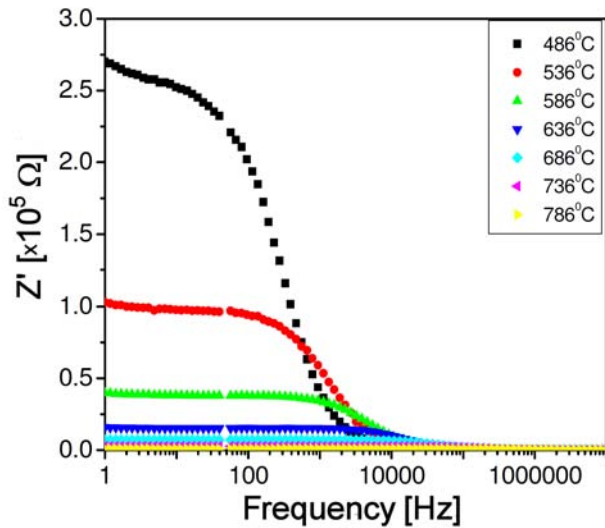


Figure 4. Frequency dependent real part of impedance at different temperatures

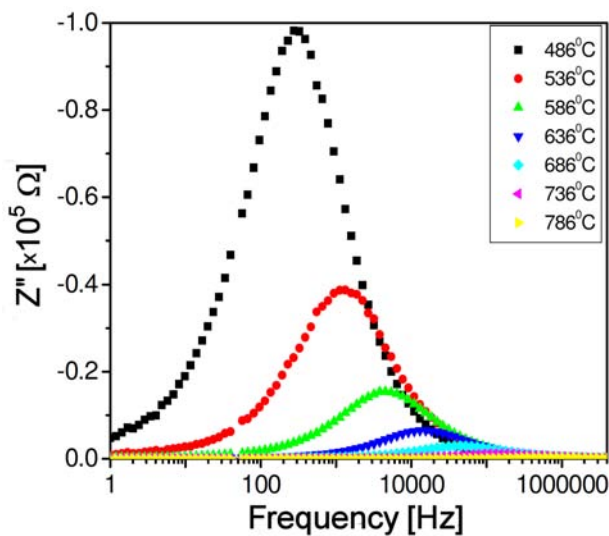


Figure 5. Frequency dependent imaginary part of impedance at different temperatures

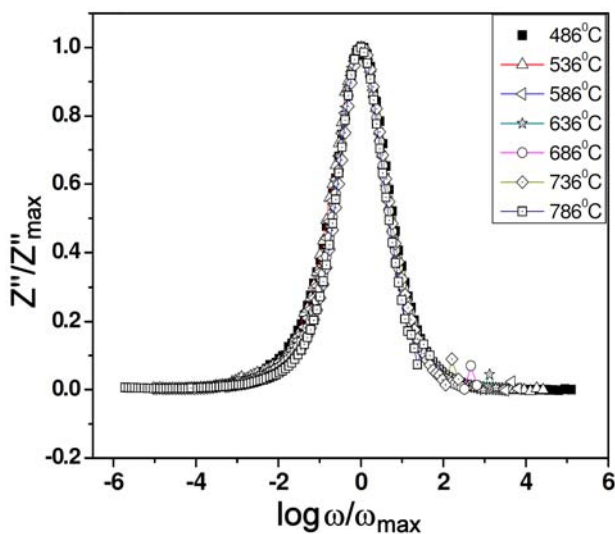


Figure 6. Scaled  $Z''(\omega, T)$  versus  $\log \omega$  [i.e.,  $Z''(\omega, T)/Z''_{max}$  and  $\log(\omega/\omega_{max})$ ]

be due to the presence of immobile species at low temperatures and defects at high temperatures. Since these observations are made at higher temperatures some relaxation species, such as defects, may be responsible for electrical conduction in the material by hopping of electrons/oxygen ion vacancies/defects among the available localized sites. The heights of peaks are found to decrease gradually with the increase in frequency and temperature, and finally, they merge in the high frequency domain. It indicates the presence of space charge polarization at lower frequencies and disappearance at higher frequencies. Figure 6 shows the plot of scaled  $Z''(\omega T)$  versus  $\log \omega$ , i.e.  $Z''(\omega T)/Z''_{max}$  and  $\log(\omega/\omega_{max})$ , where  $\omega_{max}$  corresponds to the peak frequency of the  $Z''$  versus  $\log \omega$  plots. It can be seen that the  $Z''$  data coalesced into a master curve. These observations indicate that the distribution function for relaxation times is nearly temperature independent with nonexponential conductivity relaxation.

Dielectric relaxation measurements are usually performed in the frequency domain and the data can be represented on the complex impedance plane by using the Cole-Cole function. Figure 7 shows the complex impedance spectrum for the BBT ceramic measured at different temperatures. One depressed semicircle is observed within the studied temperature range, representing the grain effect in the material. It is also observed that with the increase in temperature the radius of the semicircles decreases representing decrement in the resistivity. All the semicircles exhibit some depression degree instead of a semicircle centred at real axis  $Z'$  due to the distribution of relaxation time. The bulk resistance of the material is obtained by fitting the experimental response to that of an equivalent circuit, which is usually considered to comprise a series of one parallel Resistor-CPE (R-CPE) elements as shown in Fig. 7 (inset). The circuit parameters fitting was done by ZView software with the modelled circuits. The experimental value of bulk resistance ( $R_b$ ) at different temperatures has been

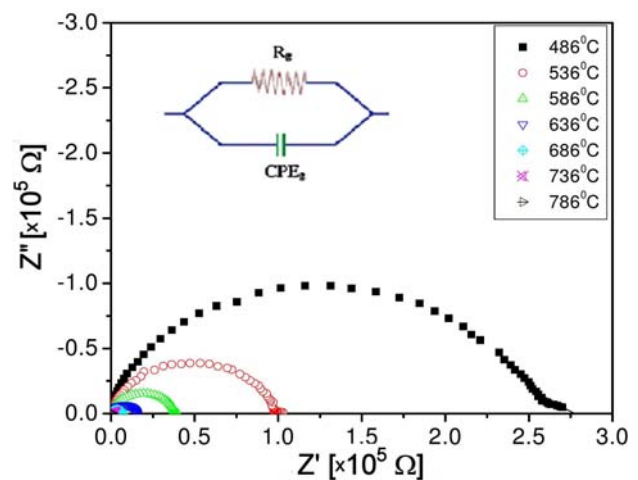


Figure 7. Nyquist plot of BBT ceramic measured at various temperatures and Inset shows the appropriate equivalent electrical circuit

obtained from the intercept of the semicircular arc on the real axis ( $Z'$ ). The depression of the semicircle is considered further evidence of polarization phenomena with a distribution of relaxation times. This can be referred to as the non-Debye type of relaxation in which there is a distribution of relaxation times [21,22]. This non-ideal behaviour can be correlated to several factors, such as grain orientation, grain boundary, stress-strain phenomena and atomic defect distribution. This modification leads to the Cole-Cole empirical behaviour described by the following equation:

$$Z^* = \frac{R}{1 + (j\omega/\omega_0)^{1-n}} \quad (2)$$

where  $n$  represents the magnitude of the departure of the electrical response from an ideal condition and can be determined from the location of the centre of the Cole-Cole circles. Least squares fitting to the complex impedance data give the value of  $n > 0$  at all the temperatures, suggesting the dielectric relaxation to be of poly-dispersive non-Debye type. This type of depressed semicircle represents a constant phase element (CPE) in the equivalent circuits. In solid materials, a distribution of relaxation times is usually observed and the capacitance is replaced by a CPE, which represents more accurately the behaviour of the grain interior, grain boundary and electrode processes [23]. From Fig. 7 it is clear that the value of  $R_b$  decreases with rise in temperature. This shows the negative temperature coefficient of resistivity (NTCR) like that of a semiconductor. The capacitances ( $C_g$ ) due to these effects can be calculated using the relation:

$$\omega_{max}RC = 1 \quad (3)$$

where  $\omega_{max} (=2\pi f_{max})$  is the angular frequency at the maxima of the semicircle. Table 1 shows the temperature variation of  $C_g$  obtained from Cole-Cole plots (using  $R_g$ ) at different temperatures.

**Table 1. Grain resistance and capacitance from Nyquist plot**

| Temperature [°C] | Resistance [ $\Omega$ ] | C [nF]   |
|------------------|-------------------------|----------|
| 486              | 286077.3                | 1.94E-09 |
| 536              | 102754.3                | 1.21E-09 |
| 586              | 39049.3                 | 8.85E-10 |
| 636              | 14526.9                 | 7.45E-10 |
| 686              | 7130.2                  | 5.40E-10 |
| 736              | 2838.7                  | 4.25E-10 |

### 3.4. Modulus analyses

The electric modulus is the reciprocal of complex permittivity and was introduced by Macedo to study the space charge relaxation process. The complex electric modulus spectrum represents the measure of the distribution ion energies or configuration in the structure and it also describes the electrical relaxation and microscopic properties. Physically the electric modulus corresponds to the relaxation of the electric field in the

material when electric displacement remains constant. The electrical response can be analysed through complex electric modulus formalism. The complex electric modulus ( $M^*$ ) has been calculated by using the relation:

$$M^*(\omega) = M' + jM'' = j\omega C_0 Z^* \quad (4)$$

where

$$M'(real\ part) = \omega C_0 Z'' \quad (5)$$

and

$$M''(imaginary\ part) = \omega C_0 Z' \quad (6)$$

where

$$C_0 = \frac{\epsilon_0 A}{t} \quad (7)$$

where  $\epsilon_0$  is permittivity in free space,  $A$  is area of electrode surface and  $t$  is thickness.

Figures 8 and 9 display the frequency (angular) dependence of  $M'(\omega)$  and  $M''(\omega)$  for BBT as a function of temperature.  $M''(\omega)$  shows a dispersion tending toward  $M_\infty$  (the asymptotic value of  $M'(\omega)$  at higher frequencies) (Fig. 8). In the low temperature region, the value of  $M'(\omega)$  increases with the increase in frequency and decreases with the rise in temperature with slow rate. While in the high-temperature region, the value of  $M'(\omega)$  increases rapidly with the increase in both the temperature and frequency [23]. It may be contributing to the conduction phenomena due to the short range mobility of charge carriers. This implies the lack of a restoring force for flow of charge under the influence of a steady electric field.

Figure 9 shows the frequency dependence of the imaginary part of the electric modulus  $M''(\omega)$  at different temperatures. The plot shows an asymmetric behaviour with respect to peak maxima whose positions

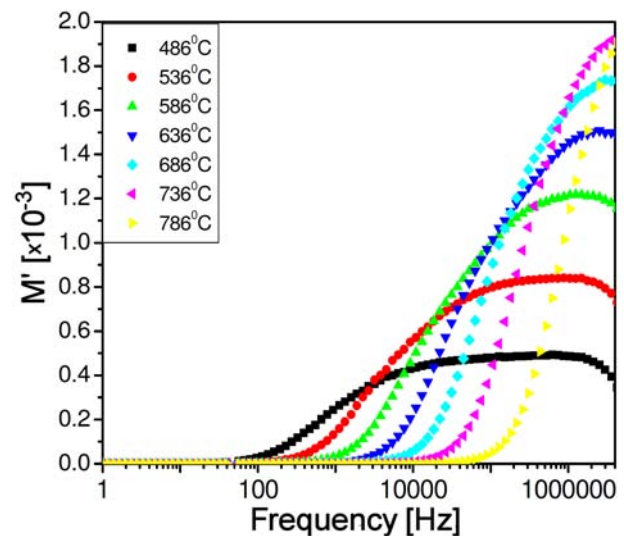


**Figure 8. Variation of real modulus with frequency at different temperature**

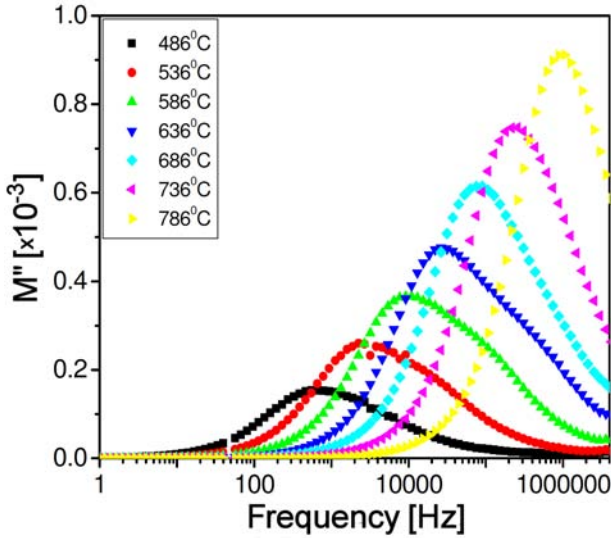


Figure 9. Variation of imaginary modulus with frequency at different temperature

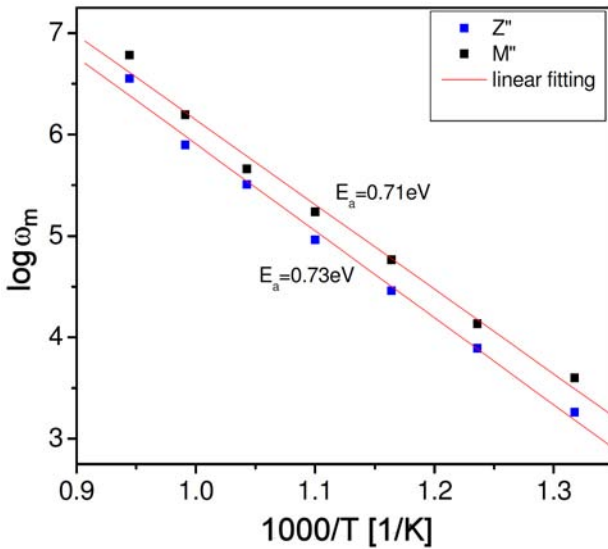


Figure 10. Arrhenius plot of  $\log \omega_m$  from imaginary part of impedance and modulus

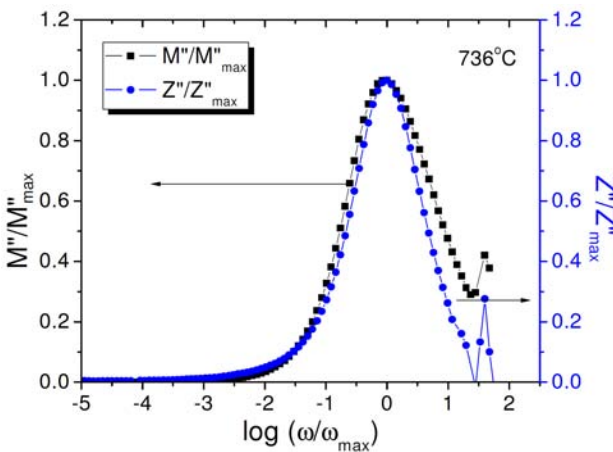


Figure 11. Frequency dependence of normalized peaks,  $Z''/Z''_{max}$  and  $M''/M''_{max}$  for the BBT ceramic at 736 °C

are frequency and temperature dependent. These spectra also reflect the motions of the ions in the material by exhibiting two apparent relaxation regions. The left regions of the peak indicate the conduction process while the right regions on the right of the peak are associated to the relaxation process where the ion can make localized motion within the well. The asymmetric modulus peaks shifts towards higher frequency side exhibiting the correlation between the motions of mobile charge carriers [24]. The asymmetry in peak broadening shows the spread of relaxation times with different time constants and hence the relaxations of non-Debye type. The existence of low frequency peaks suggests that the ions can move over long distances whereas high frequency peaks suggest about the confinement of ions in their potential well. The nature of modulus spectra confirms the existence of hopping mechanism in the electrical conduction of the materials.

The frequency  $\omega_m$  (corresponding to  $Z''_{max}$  and  $M''_{max}$ ) gives the most probable relaxation time  $\tau_m$  from the condition  $\omega_m \tau_m = 1$ . The most probable relaxation time follows the Arrhenius law given by:

$$\omega_m = \omega_0 \exp\left(\frac{-E_a}{k_B T}\right) \quad (8)$$

where  $\omega_0$  is the pre-exponential factor and  $E_a$  is the activation energy. Figure 10 shows a plot of the  $\log \omega_m$  versus  $1000/T$ , where the dots are the experimental data and the solid line is the least-squares straight-line fit of the relaxation of both  $Z''(\omega)$  and  $M''(\omega)$ . The activation energy  $E_a$  is calculated from the least-squares fit to the points. From Fig. 10 it can be seen that the activation energy, calculated from Arrhenius relation, is  $E_a = 0.73$  eV and 0.71 eV from the relaxation of  $Z''(\omega)$  and  $M''(\omega)$ , respectively.

Going further in the description of experimental data, the variations of normalized parameters  $M''(\omega)/M''_{max}$  and  $Z''(\omega)/Z''_{max}$  as a function of logarithmic frequency measured at 736 °C for BBT are shown in Fig. 11. Comparison with the impedance and electrical modulus data allows the determination of the bulk response in terms of localized, i.e. defect relaxation or non-localized conduction, i.e. ionic or electronic conductivity. Overlapping of the peak positions of the  $Z''(\omega)/Z''_{max}$  and  $M''(\omega)/M''_{max}$  is observed suggesting components from both long-range and localized relaxation. In order to mobilize the localized electron, the aid of lattice oscillation is required. In these circumstances electrons are considered not to move by them but by hopping motion activated by lattice oscillation. In addition, the magnitude of the activation energy suggests that the carrier transport is due to the hopping conduction.

### 3.5. AC/DC conductivity analyses

The AC electrical conductivity was obtained by using the relation  $\sigma_{AC} = d/(A \cdot Z')$ , where  $d$  is the thickness and  $A$  is the surface area of the material. The plot of electrical conductivity versus frequency at different

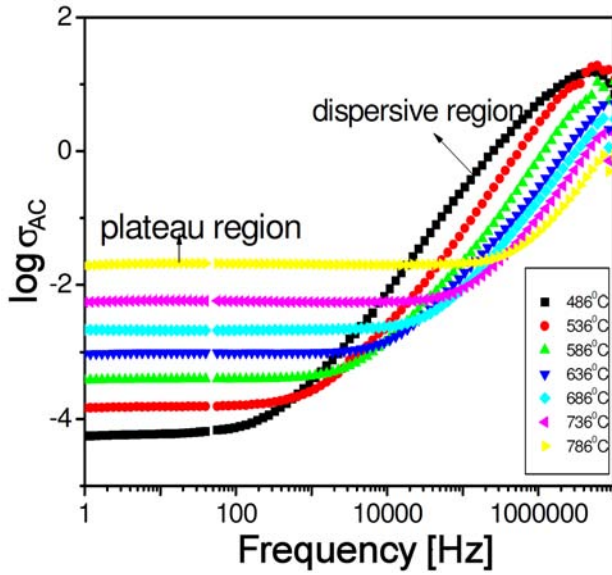


Figure 12. Variation of AC conductivity with frequency at different temperature

temperatures is shown in Fig. 12. The frequency dependence conductivity spectrum exhibits three different regions, they are: a) low frequency dispersed b) an intermediate plateau and c) conductivity dispersion at high frequencies. The variation of conductivity in the low frequency range is due to the polarisation effects [25]. At very low frequencies the accumulation of charge occurs, hence drop in conductivity. In the intermediate frequency region conductivity is almost found to be frequency independent and equal to DC conductivity in high frequency region the conductivity increases with frequency. The frequency dependence of electrical conductivity is explained by Jonscher's power law given by:

$$\sigma_{AC} = \sigma_{DC} + A\omega^n \quad (9)$$

where  $\sigma_{AC}$  is the AC conductivity,  $\sigma_{DC}$  is the limiting zero frequency conductivity,  $A$  is a pre-exponential constant,  $\omega = 2\pi f$  is the angular frequency and  $n$  is the power law exponent where  $0 < n < 1$  [26,27]. The graph indicates that the conductivity increases with increasing temperature. The conductivity is very sensitive at higher frequency known as hopping frequency, which is shifted towards higher frequency with rise in temperature. In the higher frequency the conductivity increases due to long range movement of charge carriers and the material shows the relaxor properties. It is observed that the conductivity spectra indicate the two different regions within the measured frequency range, they are a) an intermediate plateau and b) conductivity dispersion at high frequency. The intermediate plateau region corresponds to frequency independent conductivity known as DC conductivity. This region is obtained due to transport of mobile ions in response to applied electric field. The  $\sigma_{DC}$  is obtained by extrapolating to lower frequencies.

The DC conductivity estimated from the bulk response of the material has been observed as a function

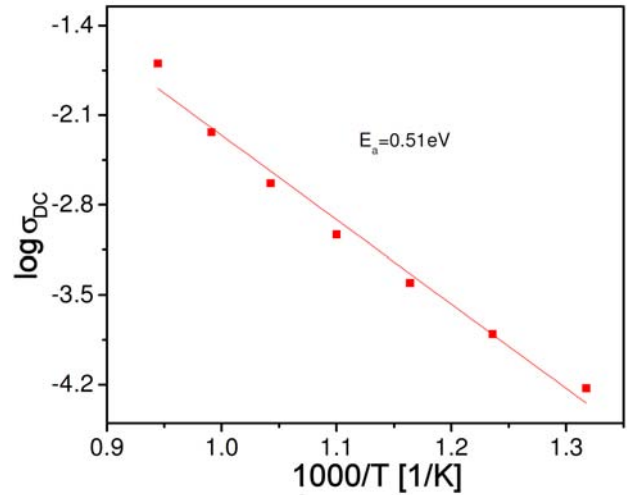
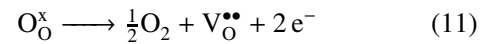


Figure 13. Temperature dependence of DC conductivity for BBT ceramic (dots are the experimental points and solid line is the least-square straight line fit)

of temperature as shown in the Fig 13. At higher temperature, the conductivity versus temperature response is linear and can be explained by a thermally activated transport of Arrhenius type governed by the relation:

$$\sigma_{DC} = \sigma_0 \exp\left(\frac{-E_a}{k_B T}\right) \quad (10)$$

where  $\sigma_0$ ,  $E_a$  and  $k_B$  represent the pre-exponential factor, the activation energy of the mobile charge carriers and Boltzmann constant respectively. The activation energy was found to be 0.51 eV. The activation energies obtained for grains is similar to the activation energy of the second ionization of oxygen vacancy in perovskites [26]. Oxygen vacancies in bismuth-layered oxides are formed by the loss of oxygen in the high-temperature sintering process, in order to balance the charge mismatch due to the existence of bismuth vacancies. In perovskite ferroelectric materials oxygen vacancies are considered to be one of the mobile charge carriers and mostly in titanates the ionization of oxygen vacancies create conduction electrons, a process which is defined by Kröger-Vink notation [28]. The excess electron and oxygen vacancies are formed in the reduction reaction:



and they may be bond to  $Ti^{4+}$  in the form  $Ti^{4+} + e^- \longleftrightarrow Ti^{3+}$ . As indicated by Ihrig and Hennings [24], it is difficult to determine whether the weakly bonded electrons are located near an oxygen vacancy or near a Ti ion. The exact location of the electrons depends on the details of structure, temperature range, etc. It was, however, shown that the oxygen vacancies lead to shallow level electrons. These electrons may be trapped by the  $Ti^{4+}$  ions or by oxygen vacancies and they easily become conducting electrons by thermal activation. The formation of oxygen vacancies can be due to the three different charge states: neutral ( $V_O^x$ ) state, which is able

to capture two electrons and it is neutral in the lattice, mono ionized ( $V_{\text{O}}^{\bullet}$ ) state and double ionized ( $V_{\text{O}}^{\bullet\bullet}$ ) state, which do not trap any electron, it is twofold positive and can be thermally activated, thus enhancing the conduction process. Double charge oxygen vacancies ( $V_{\text{O}}^{\bullet\bullet}$ ) are considered to be the major mobile charge in perovskite and play important role in conduction. Fits of the above results show that activation energies related to relaxation process are slightly higher than those related to conduction in the studied temperature range. This suggests that the relaxation process does not govern the electrical conduction. At high temperatures various types of charge carriers contribute to the electrical conduction, although these may not be related to the dielectric relaxation/polarization. For instance, the electrons released from the oxygen vacancy ionization which can be the source of the space charge polarization, are easily thermally activated and become conducting electrons. Also, dipoles related to the oxygen vacancies and electrons can be trapped easily at the grain boundaries and thus block the ionic conduction across them.

#### IV. Conclusions

Complex impedance spectroscopy has been used to study the dielectric dispersion and conduction mechanism of  $\text{BaBi}_4\text{Ti}_4\text{O}_{15}$  ceramic synthesized by solid state reaction. Impedance spectroscopy study shows a dielectric relaxation in the material which follows Maxwell-Wagner relaxations. Nyquists plots show both bulk and grain boundary effect and the resistance decreases with rise in temperature, which indicates the NTCR behaviour of the sample. The electrical relaxation process occurring in the material has been found to be temperature dependent. Modulus analysis has established the possibility of hopping mechanism for electrical transport processes in the system. The AC conductivity spectrum is found to obey Jonscher's universal power law. The frequency dependent AC conductivity at different temperatures indicated that the conduction process is thermally activated process.

#### References

1. A.Z. Simoes, B.D. Stojanovic, M.A. Ramirez, A.A. Cavalheiro, E. Longo, J.A. Varela, "Lanthanum-doped  $\text{Bi}_4\text{Ti}_3\text{O}_{12}$  prepared by the soft chemical method: Rietveld analysis and piezoelectric properties", *Ceram. Int.*, **34** (2008) 257–261.
2. J.D. Bobić, M.M. Vijatović, T. Rojac, B.D. Stojanović, "Characterization and properties of barium bismuth titanate", *Process. Appl. Ceram.*, **3** (2009) 9–12.
3. G. Nalini, T.N. Guru Row, "Structure determination at room temperature and phase transition studies above  $T_c$  in  $\text{ABi}_4\text{Ti}_4\text{O}_{15}$  ( $A = \text{Ba}, \text{Sr}$  or  $\text{Pb}$ )", *Bull. Mater. Sci.*, **25** (2002) 275–281.
4. T. Jardiell, A.C. Caballero, M. Villegas, "Aurivillius ceramics:  $\text{Bi}_4\text{Ti}_3\text{O}_{12}$ -based piezoelectrics", *J. Ceram. Soc. Jpn.*, **116** [4] (2008) 511–518.
5. G.N. Subbanna, T.N.G. Row, C.N.R. Rao "Structure and dielectric properties of recurrent intergrowth structures formed by the Aurivillius family of bismuth oxides of the formula  $\text{Bi}_2\text{A}_{n-1}\text{B}_n\text{O}_{3n+3}$ ", *J. Solid State Chem.*, **86** (1990) 206–211.
6. A. Rae, J. Thompson, R. Withers, A. Willis, "Structure refinement of commensurately modulated bismuth titanate  $\text{Bi}_4\text{Ti}_3\text{O}_{12}$ ", *Acta Cryst. B*, **46** (1990) 474–487.
7. S.K. Kim, M. Miyayama, H. Yanagida, "Electrical anisotropy and a plausible explanation for dielectric anomaly of  $\text{Bi}_4\text{Ti}_3\text{O}_{12}$  single crystal", *Mater. Res. Bull.*, **31** (1996) 121–131.
8. R.E. Newnham, R.W. Wolfe, J.F. Dorrian, "Structural basis of ferroelectricity in the bismuth titanate family", *Mater. Res. Bull.*, **6** (1971) 1029.
9. R.Z. Hou, X.M. Chen, Y.W. Zeng, "Diffuse ferroelectric phase transition and relaxor behaviors in Ba-based bismuth layer-structured compounds and La-substituted  $\text{SrBi}_4\text{Ti}_4\text{O}_{15}$ ", *J. Am. Ceram. Soc.*, **89** (2006) 2839–2844.
10. J. Tellier, Ph. Boullay, M. Manier, D. Mercurio, "A comparative study of the Aurivillius phase ferroelectrics  $\text{CaBi}_4\text{Ti}_4\text{O}_{15}$  and  $\text{BaBi}_4\text{Ti}_4\text{O}_{15}$ ", *J. Solid State Chem.*, **177** (2004) 1829–1837.
11. Ismunandar, T. Kamiyama, A. Hoshikawa, Q. Zhou, B.J. Kennedy, Y. Kubota, K. Kato, "Structural studies of five layer Aurivillius oxides:  $\text{A}_2\text{Bi}_4\text{Ti}_5\text{O}_{18}$  ( $A = \text{Ca}, \text{Sr}, \text{Ba}$ , and  $\text{Pb}$ )", *J. Solid State Chem.*, **177** (2004) 4188–4196.
12. A.V. Murugan, S.C. Navale, V. Ravi, "Preparation of nanocrystalline ferroelectric  $\text{BaBi}_4\text{Ti}_4\text{O}_{15}$  by Pechini method", *Mater. Lett.*, **60** (2006) 1023–1025.
13. D. Xie, W. Pan, "Study on  $\text{BaBi}_4\text{Ti}_4\text{O}_{15}$  nanoscaled powders prepared by sol-gel method", *Mater. Lett.*, **57** (2003) 2970–2974.
14. B.J. Kennedy, Y. Kubota, B.A. Hunter, Ismunandar, K. Kato, "Structural phase transition in the layered bismuth oxide  $\text{BaBi}_4\text{Ti}_4\text{O}_{15}$ ", *Solid State Commun.*, **126** (2003) 653–658.
15. T. Badapanda, R.K. Harichandan, A. Mishra, S. Anwar, "Relaxor ferroelectric behavior of  $\text{BaBi}_4\text{Ti}_4\text{O}_{15}$  aurivillius ceramic", *J. Adv. Dielectrics*, **3** [2] (2013) 1350013.
16. S. Kumar, K.B.R. Varma, "Dielectric relaxation in bismuth layer-structured  $\text{BaBi}_4\text{Ti}_4\text{O}_{15}$  ferroelectric ceramics", *Curr. Appl. Phys.*, **11** (2011) 203–210.
17. S. Kumar, K.B.R. Varma, "Dielectric, ferroelectric and relaxor behavior of  $\text{BaLa}_x\text{Bi}_{4-x}\text{Ti}_4\text{O}_{15}$  ceramics", *Adv. Sci. Lett.*, **3** (2010) 20–27.
18. J. Tellier, Ph. Boullay, D.B. Jennet, D. Mercurio, "Structural evolution in three and four-layer Aurivillius solid solutions: A comparative study versus relaxor properties", *J. Solid State Sci.*, **10** (2008) 177–185.

19. J. Tellier, Ph. Boullay, D.B. Jennet, D. Mercurio, “Structural versus relaxor properties in Aurivillius type of compounds”, *J. Eur. Ceram. Soc.*, **27** (2007) 3687–3690.
20. S. Kumar, K.B.R. Varma, “Relaxor behavior of  $\text{BaBi}_4\text{Ti}_3\text{Fe}_{0.5}\text{Nb}_{0.5}\text{O}_{15}$  ceramics”, *Solid State Commun.*, **147** (2008) 457–460.
21. T. Kimura, Y. Yoshida, “Origin of texture development in barium bismuth titanate prepared by template grain growth method”, *J. Am. Ceram. Soc.*, **89** (2006) 869–874.
22. M. Suzuki, M. Miyayama, Y. Noguchi, T. Uchikoshi, “Enhanced piezoelectric properties of grain-oriented  $\text{Bi}_4\text{Ti}_3\text{O}_{12}$ – $\text{BaBi}_4\text{Ti}_4\text{O}_{15}$  ceramics obtained by magnetic-field-assisted electrophoretic deposition method”, *J. Appl. Phys.*, **104** (2008) 014102.
23. I. Pribosic, D. Makovec, M. Drogenik, “Electrical properties of donor and acceptor doped  $\text{BaBi}_4\text{Ti}_4\text{O}_{15}$ ”, *J. Eur. Ceram. Soc.*, **21** (2001) 1327–1331.
24. T. Kobayashi, Y. Noguchi, M. Miyayama, “Enhanced spontaneous polarization in super lattice structure  $\text{Bi}_4\text{Ti}_3\text{O}_{12}$ – $\text{BaBi}_4\text{Ti}_4\text{O}_{15}$  single crystal”, *Appl. Phys. Lett.*, **86** (2005) 012907.
25. A. Chakrabarti, J. Bera, T.P.Sinha, “Dielectric properties of  $\text{BaBi}_4\text{Ti}_4\text{O}_{15}$  ceramic produced by cost-effective chemical method”, *Physics B*, **404** (2009) 1498–1502.
26. H. Du, Y. Li, H. Li, X. Shi, C. Liu, “Relaxor behavior of bismuth layer-structured ferroelectric ceramic with”, *Solid State Commun.*, **148** (2008) 357–360.
27. A.K. Jonscher, “Dielectric relaxation in solids”, *J. Mater. Sci.*, **16** (1981) 2037–2060.
28. C. Ang, Z. Yu, Z. Jing, P. Lunkenheimer, A. Loidl, “Dielectric spectra and electrical conduction in Fe-doped  $\text{SrTiO}_3$ ”, *Phys. Rev. B*, **61** (2000) 3922–3926.